Journal of Earth Science, *Vol. 20*, *No. 3*, *p. 563–579*, *June 2009* *ISSN 1674-487X*
Printed in China
DOI: 10.1007/s12583-009-0047-7

High-Frequency Rayleigh-Wave Method

Jianghai Xia*, **Richard D Miller**
Kansas Geological Survey, *The University of Kansas*, *Lawrence*, *KS* 66047, *USA*
Xu Yixian (徐义贤), **Luo Yinhe** (罗银河), **Chen Chao** (陈超), **Liu Jiangping** (刘江平)
Institute of Geophysics and Geomatics, *China University of Geosciences*, *Wuhan* 430074, *China*
Julian Ivanov, **Chong Zeng**
Kansas Geological Survey, *The University of Kansas*, *Lawrence*, *KS* 66047, *USA*

ABSTRACT: High-frequency (≥2 Hz) Rayleigh-wave data acquired with a multichannel recording system have been utilized to determine shear (S)-wave velocities in near-surface geophysics since the early 1980s. This overview article discusses the main research results of high-frequency surface-wave techniques achieved by research groups at the Kansas Geological Survey and China University of Geosciences in the last 15 years. The multichannel analysis of surface wave (MASW) method is a non-invasive acoustic approach to estimate near-surface S-wave velocity. The differences between MASW results and direct borehole measurements are approximately 15% or less and random. Studies show that simultaneous inversion with higher modes and the fundamental mode can increase model resolution and an investigation depth. The other important seismic property, quality factor (*Q*), can also be estimated with the MASW method by inverting attenuation coefficients of Rayleigh waves. An inverted model (S-wave velocity or *Q*) obtained using a damped least-squares method can be assessed by an optimal damping vector in a vicinity of the inverted model determined by an objective function, which is the trace of a weighted sum of model-resolution and model-covariance matrices. Current developments include modeling high-frequency Rayleigh-waves in near-surface media, which builds a foundation for shallow seismic or Rayleigh-wave inversion in the time-offset domain; imaging dispersive energy with high resolution in the frequency-velocity domain and possibly with data in an arbitrary acquisition geometry, which opens a door for 3D surface-wave techniques; and successfully separating surface-wave modes, which provides a valuable tool to perform S-wave velocity profiling with high-horizontal resolution.

KEY WORDS: Rayleigh wave, dispersion, high mode, mode separation, seismic modeling, model appraisal.

INTRODUCTION

Surface waves are guided and dispersive. Rayleigh waves are surface waves that travel along a "free" surface, such as the earth-air or the earth-water interface, and are usually characterized by relatively low velocity, low frequency, and high amplitude (Sheriff, 2002). Rayleigh waves are the result of interfering P and S_v waves. Particle motion of the fundamental mode of Rayleigh waves in a homogeneous medium moving from left to right is elliptical in a counter-clockwise (retrograde) direction along the free surface. As depth increases, the particle motion becomes prograded and is still elliptical when reaching

This study was supported by Kansas Geological Survey, The University of Kansas and China University of Geosciences.
*Corresponding author: jxia@kgs.ku.edu

Manuscript received October 31, 2008.
Manuscript accepted December 17, 2008.

sufficient depth. The motion is constrained to a vertical plane consistent with the direction of wave propagation. For the case of a solid homogenous half-space, the Rayleigh wave is not dispersive and travels at a velocity of approximately 0.919 4V_S when Poisson's ratio is equal to 0.25, where V_S is the S-wave velocity of the half-space (Sheriff and Geldart, 1983). However, in the case of one layer over a solid homogenous half-space, Rayleigh waves become dispersive when their wavelengths are in the range of 1 to 30 times the layer thickness (Stokoe et al., 1994). Longer wavelengths penetrate greater depths for a given mode, generally exhibit greater phase velocities, and are more sensitive to the elastic properties of the deeper layers (Babuska and Cara, 1991). Conversely, shorter wavelengths are sensitive to the physical properties of surface layers. Therefore, a particular mode of surface wave will possess a unique phase velocity for each unique wavelength, leading to the dispersion of surface waves.

Shear (S)-wave velocities can be derived by inverting the dispersive phase velocity of the surface (Rayleigh and/or Love) wave (e.g., Dorman and Ewing, 1962). Near-surface S-wave velocity can also be determined by inverting high-frequency Rayleigh waves. Several seismic methods utilize dispersion of Rayleigh waves to determine S-wave velocities of near-surface materials. Stokoe and Nazarian (1983) and Nazarian et al. (1983) presented a surface-wave method, spectral analysis of surface wave (SASW), which analyzes the dispersion curve of Rayleigh waves to produce near-surface S-wave velocity profiles. Matthews et al. (1996) summarized the SASW method and the continuous surface wave (CSW) method (Tokimatsu et al., 1991; Abbiss, 1981) with detailed diagrams. For the last 15 years, the Kansas Geological Survey (KGS) at The University of Kansas has developed a method called multichannel analysis of surface waves (MASW), which can be traced back to the work by Song et al. (1989). The method includes acquisition of high-frequency (≥2 Hz) broadband Rayleigh waves, extraction of Rayleigh- wave dispersion curves from Rayleigh waves, and inversion of dispersion curves to obtain near-surface S-wave velocity profiles. The MASW method has been given increasingly more attention by the near-surface geophysical community with application to a variety of near-surface geological and geophysical problems because it is non-destructive, non-invasive, low cost, and relatively highly accurate. It becomes a main tool in determining S-wave velocities for applications of near-surface geology, environment, and engineering.

The elastic properties of near-surface materials and their effects on seismic-wave propagation are of fundamental interest in groundwater, engineering, environmental studies, and petroleum exploration. S-wave velocity is a key parameter in construction engineering. As an example, Imai and Tonouchi (1982) studied P- and S-wave velocities in an embankment, and also in alluvial, diluvial, and Tertiary layers, showing that S-wave velocities in such deposits correspond to the N-value (blow count; Clayton et al., 1995; Clayton, 1993), an index value of formation hardness in soil mechanics and foundation engineering. S-wave velocity is also an important parameter for evaluating the dynamic behavior of soil in the shallow subsurface (Yilmaz et al., 2006). For example, both the Uniform Building Code (UBC) and Eurocode 8 (EC8) codes use V_S^{30}, the average S-wave velocity for the top 30 m of soil, to classify sites according to the soil type for earthquake-engineering design purposes (Sabetta and Bommer, 2002; Sêcoe and Pinto, 2002; Dobry et al., 2000). In petroleum exploration, a near-surface layer acts as a filter that smears images of deep reflection events. To eliminate the smearing effect, accurate near-surface velocity information is critical. However, to determine near-surface velocities is a troublesome task, especially for S-wave reflection/refraction survey. As discussed by Xia et al. (2002b, 1999), one successful alternative of determining S-wave velocities of near-surface layers is to use the MASW method.

Researchers at the KGS applied the MASW method to solve numerous geological, environmental, and engineering problems, and also analyzed the effects of higher modes on inversion of surface waves and investigation depth, the feasibility of estimating near-surface quality factor (Q) by inverting attenuation coefficients of Rayleigh waves, and applications of data-resolution and model-resolution matrices in surface-wave data, etc.. For the past five years, researchers from the Institute of Geophysics and Geo-

matics at China University of Geosciences have worked closely with researchers at the KGS and developed techniques of forward modeling, generation of high-resolution images in the *f*-*v* domain, mode separation, and increase of horizontal resolution of surface-wave techniques. In this article, our discussion will mainly focus on the fundamentals and recent developments of the MASW method carried out by these two groups.

NEAR-SURFACE SEISMIC PROPERTIES

Rayleigh waves travel along or near the ground surface and are usually characterized by relatively low velocity, low frequency, and high amplitude. The main characteristic of surface waves is dispersive, which means that their velocities change with frequency and are mainly affected by S-wave velocities. A method proposed by Song et al. (1989) utilizes a multichannel recording system to estimate near-surface S-wave velocities using high-frequency surface waves. A systematic research project on using MASW to determine near-surface S-wave velocities was launched in the early 1990s at the KGS. The principal advantages of the MASW method are ease in recognizing surface waves (both the fundamental and higher modes), eliminating the body-wave energy, defining phase velocities of surface waves, and obtaining accurate S-wave velocities. The seismic properties of near-surface materials are P- and S-wave velocities, P-wave quality factor Q_P, and S-wave quality factor Q_S. In the following sections, we will discuss the main steps (Fig. 1) of the MASW method from a shot gather to an S-wave velocity profile (S-wave velocity vs. depth) and show an approach determining Q_S using amplitudes of Rayleigh waves.

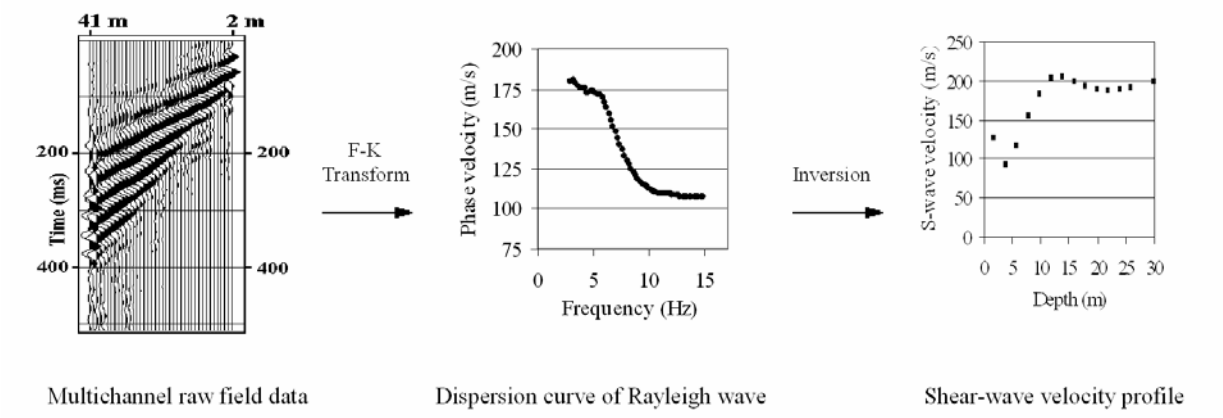

Figure 1. A diagram of the MASW method (Xia et al., 2004a). Multichannel raw field data, which contain enhanced Rayleigh-wave signals, are first acquired. Rayleigh-wave phase velocity is then extracted from the field data in the *f*-*v* domain. The phase velocity, finally, is inverted for a shear-wave velocity profile (V_S vs. depth).

Surface-Wave Data Acquisition

The equipment and instruments used in surface-wave data acquisition are almost the same as used in the shallow-reflection survey except for receivers. To record wide-bandwidth surface waves, low-frequency receivers, normally 4.5 Hz, are used in the investigation of the subsurface up to 30 m depth. Sledgehammers (6 kg or so), weight droppers, and vibrators are good non-invasive seismic sources for surface-wave surveys. A 24-, 48-, or 60-channel seismograph is suitable for recording surface-wave data.

Optimal recording of Rayleigh waves also requires field configurations and acquisition parameters favorable to recording planar Rayleigh waves. Depending on an investigation depth, Rayleigh waves with certain wavelengths need a certain amount of time to be developed into planar waves. Plane-wave propagation of surface waves does not occur in most cases until the near-offset (distance between the source and the first receiver) is greater than half the maximum desired wavelength (Stokoe et al., 1994). Numerous articles discuss the theoretical and empiri-

cal approaches determining optimal data-acquisition parameters (e.g., Xia et al., 2006a, 2004a; Xu et al., 2006; Zhang et al., 2004). The maximum penetration depth in a homogeneous medium is about one wavelength. The currently accepted rule of thumb of the maximum penetration depth is approximately half the longest wavelength (Rix and Leipski, 1991). Higher modes, however, can penetrate deeper than one wavelength (Xia et al., 2003). The near-offset distance should be selected as almost the same as the investigation depth. High-frequency surface waves attenuate quite rapidly with distance away from the source so body waves may also contaminate the surface-wave data recorded by receivers at far offsets (Park et al., 1999). To acquire dominant high-frequency components in the further offsets, the far-offset (the distance between the source and the furthest receiver) is normally selected as a distance that is twice the investigation depth. A dispersion image in the frequency-velocity (*f*-*v*) domain is affected by a receiver spread. The resolution of a dispersion image is directly proportional to the product of the receiver spread and the frequency [Forbriger, 2003; d=1/fC, where d is the half-width between the neighboring minima of dispersion energy in the frequency-slowness (f-1/v) domain; f is the frequency; and C is the receiver spread]. Normally, the longer the geophone spread is, the higher the resolution of the dispersion image. To avoid spatial aliasing, the receiver spacing should not be larger than half the shortest wavelength measured. Basically, after knowing the investigation depth for a particular problem, a practical rule of determining data-acquisition parameters: the nearest offset (A), receiver spacing (B), and receiver spread (C), is shown in Fig. 2.

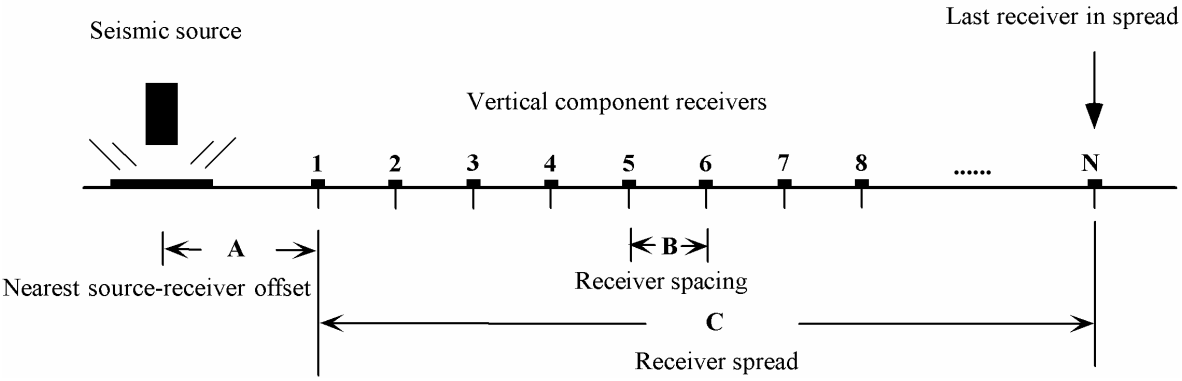

Figure 2. Three field-data-acquisition parameters (Xia et al., 2004a). *A*. The nearest source-receiver offset: approximately equal to the maximum investigation depth; *B*. receiver spacing: the thinnest layer of the layer model; *C*. receiver spread—distance between the first receiver and the last receiver: about 2 times the maximum investigation depth.

Studies on fast and efficient methods for surface-wave data acquisition were carried out by several research groups. Miller et al. (1999) demonstrated that streamer data could be acquired by surface waves with the same quality as by planted receivers. Tian et al. (2003a, b) utilized geophone-deployment equipment, autojuggie (Steeples et al., 1999), with the MASW method in subsurface mapping, and discussed a special data-sorting approach.

Dispersion Curves

Generating a reliable image of dispersion energy in the *f*-*v* domain is a key step in the MASW method. Xia et al. (2007a) developed an algorithm that can be applied to data acquired with receivers in an arbitrary acquisition geometry, which consists of two steps: (1) the frequency decomposition (Coruh, 1985), stretching multichannel impulsive data $x(d, t)$ (d is an offset) into pseudo-vibroseis data or frequency-swept data $X(d, t)$ by a convolution operation $X(d, t) = S(t) * x(d, t)$, where $*$ stands for the convolution operation; and $S(t)$ is a linear or non-linear sweep and should cover a frequency range of interest; and (2) slant stacking frequency-swept data (Yilmaz, 1987). Due to the flexibility of receivers' layout, this method presents a solution to 3D S-wave velocity mapping using

Rayleigh waves. Luo et al. (2008a) proposed to image Rayleigh-wave dispersive energy by high-resolution linear radon transform (LRT). The shot gather is first transformed along the time direction to the frequency domain and then the Rayleigh-wave dispersive energy can be imaged by high-resolution LRT using a weighted preconditioned conjugate gradient algorithm. Before the works of Xia et al. (2007a) and Luo et al. (2008a), three algorithms were available in calculating image of high-frequency dispersion energy: the *F-K* transformation (e.g., Yilmaz, 1987), the τ-*p* transform (McMechan and Yedlin, 1981), and the phase shift (Park et al., 1998). Moro et al. (2003) evaluated the effectiveness of three computational schemes for phase-velocity computation based on *F-K* spectrum, τ-*p* transform, and phase shift. They concluded that the phase-shift approach is insensitive to data processing and performs very well even when a limited number of traces are considered.

The resolution of the peaks is the key to obtaining an accurate dispersion curve. Synthetic and real-world examples demonstrated that the resolution of dispersion images generated by high-resolution LRT is 50% higher than other methods (Luo et al., 2008a). A locus along peaks of dispersion energy over different values of frequencies in the *f*-*v* domain permits the images of dispersion curves to be constructed.

Inversion of Dispersion Curves

A layered-earth model is commonly used in solving a 1-D problem. The Rayleigh-wave phase velocity of the layered-earth model is a function of frequency and four groups of earth properties: P-wave velocity, S-wave velocity, density, and thickness of layers. Analysis of the Jacobian matrix provides a measure of dispersion-curve sensitivity to the earth properties (Xia et al., 1999). S-wave velocity is the dominant influence on a dispersion curve in a high-frequency range ($\geq$ 2 Hz); so only S-wave velocities are unknown in current inversion. An iterative solution to the weighted equation (Xia et al., 1999) proved very effective in the high-frequency range when using the Levenberg-Marquardt (L-M) method (Marquardt, 1963). Convergence of the solution is guaranteed and stable through the selection of an initial model (Xia et al., 1999) and the damping factor of the L-M method.

The only continuous model, a compressible Gibson half-space, currently used in near-surface geophysics, is the shear modulus varying linearly with depth in an inhomogeneous elastic half-space (Xia et al., 2006b). An analytical dispersion law of Rayleigh-type waves in a compressible Gibson half-space is in an algebraic form (Vardoulakis and Verttos, 1988), which makes our inversion processing extremely simple and fast (Xia et al., 2006b). This is useful in practice where Rayleigh-wave energy is only developed in a limited frequency range or at certain frequencies as data acquired at manmade structures such as dams and levees. This model can also be used in defining a good initial model for other iterative algorithms.

Specific treatments may be given for the subsurface with a high-velocity layer (HVL) or a low-velocity layer (LVL). Carefully selecting an initial model is required for a meaningful solution as discussed by Calderón-Macías and Luke (2007) on surface-wave inversion with an HVL intrusion model. In that case, an HVL should be characterized in an initial model to obtain meaningful results. Lu et al. (2007) demonstrated that the apparent discontinuity is caused by a rapid change of mode excitation with frequency at the surface. While one mode vanishes from the recorded wavefield, the other appears. This indicates that the surface displacements of the modes should also be accounted for in the inverse problem, especially in stratified media with an LVL. Modeling results (Liang et al., 2008) also indicated that Rayleigh-wave phase velocities possess the lowest sensitivity to the layer above the LVL.

Verification

Systematic verification of inverted S-wave velocities from Rayleigh-wave inversion was completed in various sites in North America in the later 1990s. S-wave velocity profiles derived from MASW compared favorably with direct borehole measurements at sites in Kansas (Xia et al., 1999); Vancouver, Canada (Xia et al., 2002a); and Wyoming (Xia et al., 2002b). The effects of changing the total number of recording channels, sampling interval, source offset, and receiver spacing on the inverted S-wave velocity were studied at a test site in Lawrence, Kansas. On the av-

erage, the difference between MASW-calculated V_S and borehole-measured V_S in eight wells along the Fraser River in Vancouver, Canada, was less than 15%. One of the eight wells was a blind test well with the calculated overall difference between MASW and borehole measurements less than 9%. No systematic differences were observed in derived V_S values from any of the eight test sites.

Surface-wave data (Fig. 3a) were collected in Wyoming after an SH refraction survey failed to produce near-surface S-wave velocities (Xia et al., 2002b). Multichannel records were acquired off both ends of a profile. A dispersion image (Fig. 3b) from the shot gather on the left panel (Fig. 3a) was generated by high-resolution LRT (Luo et al., 2008a). The fundamental mode of Rayleigh waves was dominated in the *f-v* domain (Fig. 3b) so phase velocities were easily determined. Initial S-wave velocities were determined from the dispersion curve based on the formula in Xia et al. (1999). The inverted S-wave velocities from the MASW method were confirmed by the results of a suspension log drilled on the site (Fig. 4). In the depth range of 0 to 6 m, the average difference between S-wave velocities estimated from the MASW method and those measured from suspension logging was less than 15%. If a 5-point moving-average filter was applied to the suspension-log data to reduce the obvious measurement noise, the general trend of linearly increasing velocity with depth of both data sets should have been approximately the same in the range of 6 to 14 m. S-wave velocities represented by the solid line (Fig. 4) were determined by the SH-refraction survey. It was obvious that S-wave velocities from the SH refraction were too high compared with the V_S from the suspension log. Xia et al. (2002b) confirmed that the velocities determined by the SH refraction were actually converted P-wave velocities after a P-wave refraction survey was conducted.

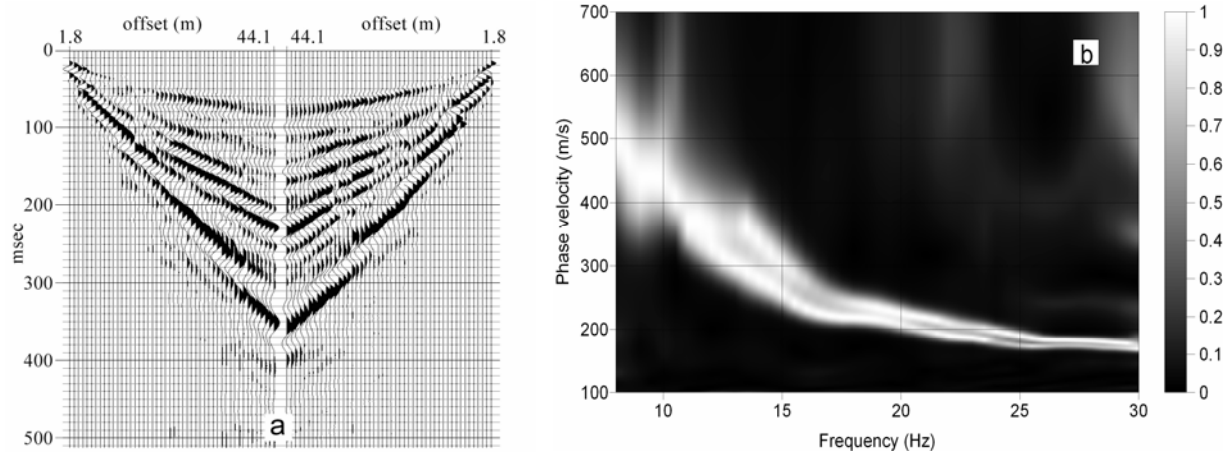

Figure 3. (a) Forty-eight-channel surface-wave data (Xia et al., 2002b) acquired off both ends of a W-E line in Wyoming using 8-Hz vertical-component geophones that were deployed at 0.9-m intervals with the nearest offset of 1.8 m. The source was a 6.3-kg hammer vertically impacting a metal plate; (b) a dispersion image in the *f-v* domain from the raw data shown in the left panel of Fig. 3a.

Near-Surface *Q*

The quality factor (Q) as a function of depth, which is directly related to the material damping ratio D ($=0.5Q^{-1}$) (Rix et al., 2000), is of fundamental interest in geotechnical engineering, groundwater, and environmental studies, as well as in oil exploration and earthquake seismology. A desire to understand the attenuative properties of the earth is based on the observations that seismic-wave amplitudes are reduced as waves propagate through an elastic medium. The modeling results (Xia et al., 2002c) suggest that it is feasible to solve for P-wave quality factor Q_P and S-wave quality factor Q_S in a layered-earth model by inverting Rayleigh-wave attenuation coefficients when V_S/V_P reaches 0.45. Only Q_S can be estimated from Rayleigh-wave attenuation coefficients when V_S/V_P is less than 0.45. The sensitivity analysis showed that errors in inverted quality factors could reach 1 to 1.5

times the error in attenuation coefficients. Compared with the inversion system for Rayleigh waves (Xia et al., 1999; 10% error in surface-wave phase velocity will result in 6% error in S-wave velocity), the inversion system for Q (Xia et al., 2002c) possesses less stability. Hence, accurate calculation of Rayleigh-wave attenuation coefficients is critical. On the other hand, the inversion system for Q is more stable than the AVO (amplitude versus offset) analysis studied and practiced in the oil industry for the last 20 years. It is known that in AVO analysis, a 10% error in incident angles could result in a 40% error in reflection coefficients (Jin et al., 2000). Xia et al. (2002c) used an algorithm (Menke, 1984) with a modification of introducing a damping factor to solve Q_P and/or Q_S from attenuation coefficients of Rayleigh waves.

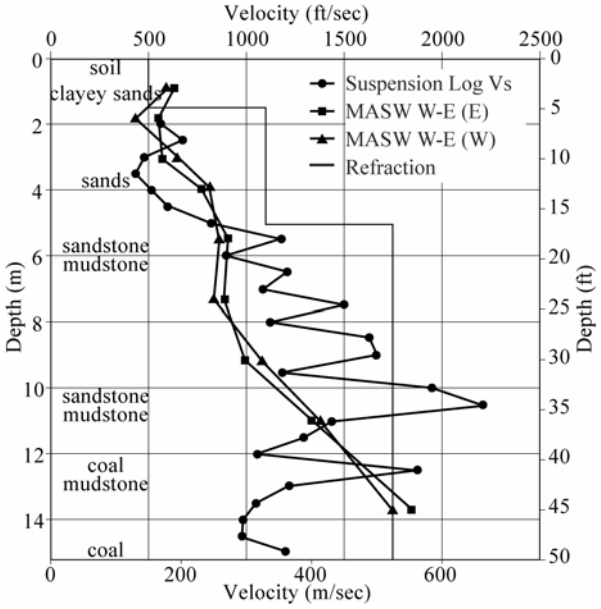

Figure 4. S-wave velocities from inverted S-wave velocities labeled as MASW W-E (E) and MASW W-E (W) and the suspension log. Labels (E) or (W) indicate the source at the east or west end of the survey line, respectively (Fig. 3a). The three-layer velocity model derived from the SH refraction survey is also presented by a solid line, labeled as refraction (from Xia et al., 2002b).

A successful example is the data (Fig. 5a) acquired in the Arizona desert. S-wave velocities (Fig. 5b) of a 10-layer model were calculated by the MASW method with known P-wave velocities. Attenuation coefficients of Rayleigh waves (Fig. 5c) were calculated by the definition of amplitude attenuation. Data denoted "Measured" were calculated from raw data and those labeled "Final" were calculated based on the inverted quality factor model (Fig. 5d). Q factors in up 20 m (Fig. 5d) were found based on the Rayleigh-wave attenuation coefficients (Fig. 5c). Q_S was in the range of 7–25. Q_P was assumed twice as large as Q_S. Modeled Rayleigh-wave attenuation coefficients (labeled "Final" in Fig. 5c) matched well with the measured coefficients.

IMPROVEMENT AND APPRAISAL OF S-WAVE VELOCITIES

Studies show that accuracy of inverted S-wave velocities can be improved significantly by inversion of the fundamental data with higher modes simultaneously, and error bars associated with those velocities can be calculated using a concept of a trade-off between model resolution and variance.

Higher Modes

A series of Rayleigh waves of different frequencies can have the same wave velocity. These different-frequency Rayleigh waves for a given phase velocity are known as modes and are characterized by their different numbers of horizontal nodal planes (planes of no particle displacement within the layer; Garland, 1979). In other words, more than one phase velocity can be associated with a given frequency of Rayleigh waves simply because these waves can travel at different velocities for a given frequency. The lowest velocity for any given frequency is called the fundamental-mode velocity (or the first mode). The next velocity higher than the fundamental-mode phase velocity is called the second-mode velocity, and so on. All phase velocities that are higher than the fundamental-mode velocities are called higher modes.

Most surface-wave researchers are also aware that the accuracy of the inverted S-wave velocity can be significantly improved by the incorporation of higher-mode data when available (Liang et al., 2008; Luo et al., 2007; Song and Gu, 2007; Xia et al., 2003, 2000; Beaty et al., 2002). Xia et al. (2003, 2000) identified two quite significant higher-mode properties through analysis of the Jacobian matrix populated with high-frequency Rayleigh-wave data. First, for

fundamental- and higher-mode Rayleigh wave data with the same wavelength, higher-mode Rayleigh waves can penetrate deeper than the fundamental mode. Second, higher-mode data can increase resolution of inverted S-wave velocities. In addition, their modeling results demonstrated that P-wave velocities affect higher modes much less than the fundamental mode, which provides a basis that inversion of higher modes could produce better S-wave velocities.

High-frequency surface-wave data (Fig. 6a) were acquired in San Jose, California, to determine shear-wave velocities of near-surface materials up to 10 m deep. Note the dispersion-curve image (Fig. 6b) in the *f-v* domain where high modes are obvious. The second mode is from 20 to 50 Hz and the third mode starts at 35 Hz. Three data sets were generated and inverted for comparison. The first set was fundamental-mode surface-wave data only, automatically extracted from Fig. 6b by SurfSeis© (a commercial software package developed at the KGS). The second data set was fundamental-mode data with noise deliberately introduced in the frequency range from 13 to 19 Hz. Noises were determined experimentally to simulate a case where the fundamental-mode data are contaminated with higher modes and/or body waves. Based on our experience, the shape of the second data set as shown here is commonly seen in real dispersion curves. The standard deviation between these two data

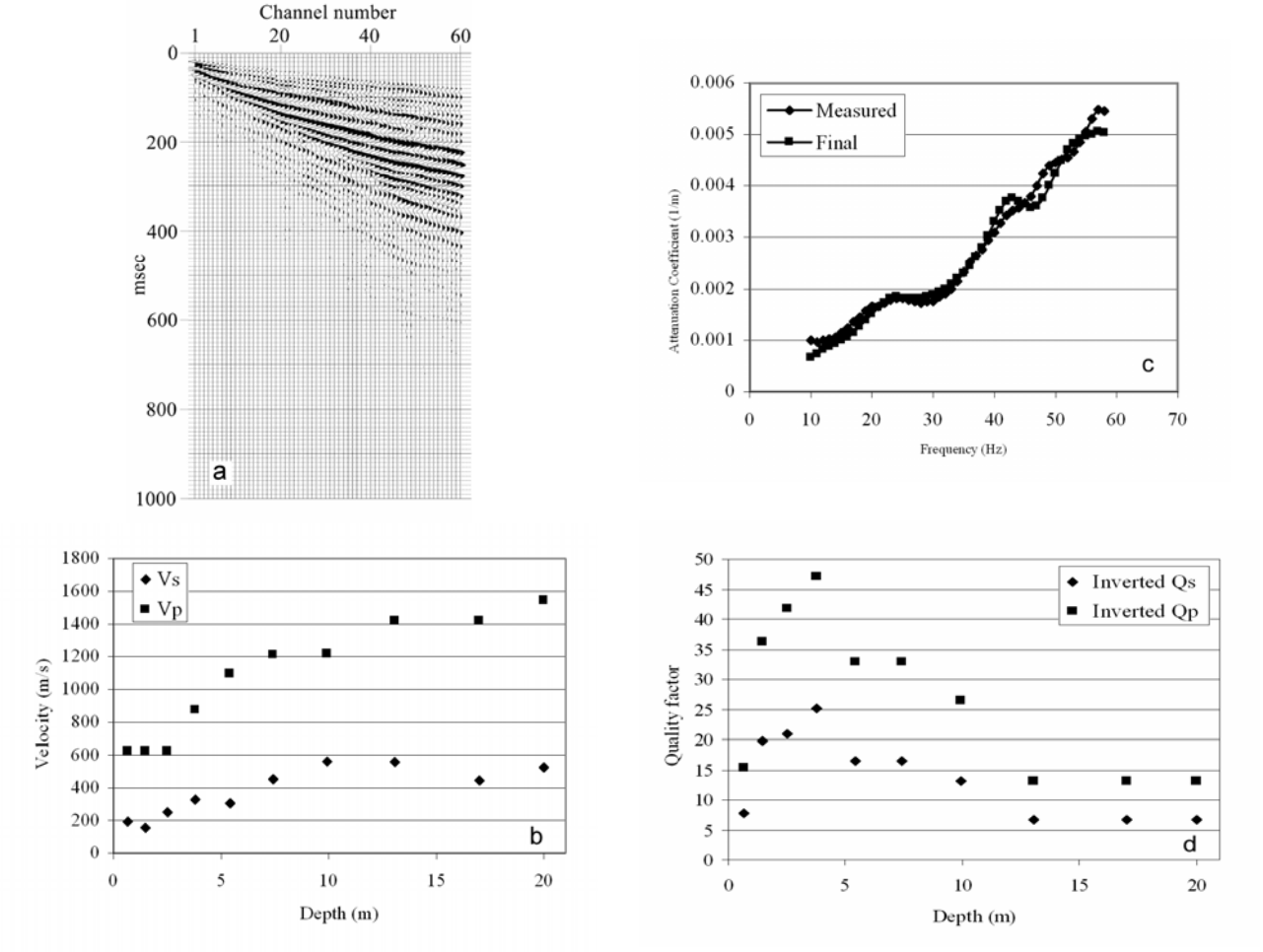

Figure 5. An example from the Arizona desert (Xia et al., 2002c). (a) Sixty-channel surface-wave data acquired using 4.5-Hz vertical geophones that were deployed at 1.2-m intervals with the nearest offset of 4.8 m. The seismic source was an accelerated weight drop designed and built by the KGS; (b) inverted S-wave velocities of a 10-layer model by the MASW method and known P-wave velocities; (c) measured and modeled Rayleigh-wave attenuation coefficients. Data with "Measured" were calculated from raw data and those labeled "Final" were calculated based on the inverted quality factor model (d).

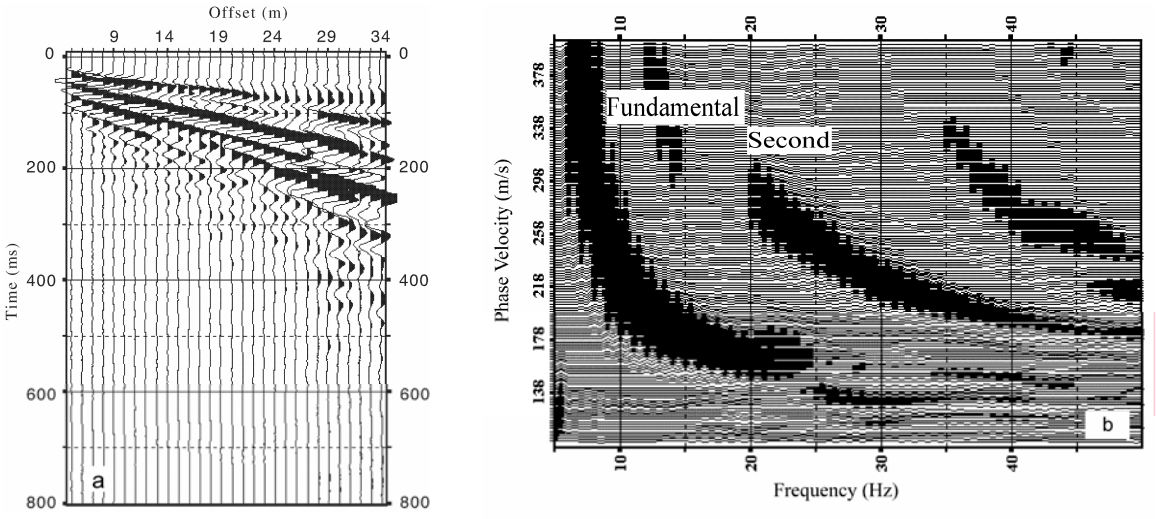

Figure 6. An example from San Jose, California (Xia et al., 2003). (a) Raw surface-wave data were acquired by using thirty 4.5-Hz vertical-component geophones with a 1-m receiver interval and the nearest offset of 4 m. The source was a 6.3-kg hammer vertically impacting a metal plate; (b) data image in the *f-v* domain.

sets is only 16 m/s. The third data set included the second set (noisy data) and the second-mode surface-wave data. A 14-layer model with each layer 1 m thick was chosen to test these three data sets.

Figure 7a shows inverted S-wave velocities from all three data sets. All root-mean-square (rms) errors between the measured-dispersion curves and calculated-dispersion curves from each of these S-wave velocity models (Fig. 7a) are less than 5 m/s. Because the fundamental-mode data (the first data set) were accurately extracted from Fig. 6b, the inverted S-wave velocities (solid squares in Fig. 7a) were geologically reasonable. They smoothly increase from shallower layers to deeper layers. However, smoothness disappears when the second data set was inverted. The S-wave velocity model (diamonds with a solid line in Fig. 7a) changes irrationally in the depth range from 3 to 7 m. This instability is caused by forcing the response of the inverted model to fit the noise.

In the real world, it is common to provide an error threshold that could force an inverted model into an unreasonable space. We have experienced this situation a number of times when processing surface-wave data. Better results are obtained when higher-mode surface-wave data (the third data set) are inverted simultaneously with the fundamental-mode data. Because of the higher rms error in the calculated second-mode data, the S-wave velocity model with abrupt variation (diamonds with a solid line in Fig. 7a) was rejected. Inverted S-wave velocities (solid triangles in Fig. 7a) that included the second modes during inversion were similar to the results obtained from the first data set (solid squares in Fig. 7a). The inversion process is more stable when including higher-mode data in the inversion of surface-wave data. This stability indeed improves the resolution of inversion results.

So what should we do if no higher modes are available? We have to make a choice between error and resolution of the inverted model. A trade-off between error and resolution of a model to obtain stable results is a wise strategy (Backus and Gilbert, 1970). We can reduce errors in the inverted S-wave velocity model by reducing the resolution of the model (increasing thickness of layers). In the San Jose example, we inverted the second data set again with a seven-layer model, each layer being 2 m thick. This model possesses only half the resolution of the previous model (a 1-m-thick model in Fig. 7a). The second data set underwent the same inversion procedure used for the San Jose example. Clearly, the inverted S-wave velocity model with the reduced resolution (a 2-m-thick model, diamonds with a solid line Fig. 7b) was smoother and geologically more acceptable than the inverted mode depicted by diamonds with a solid line (Fig. 7a).

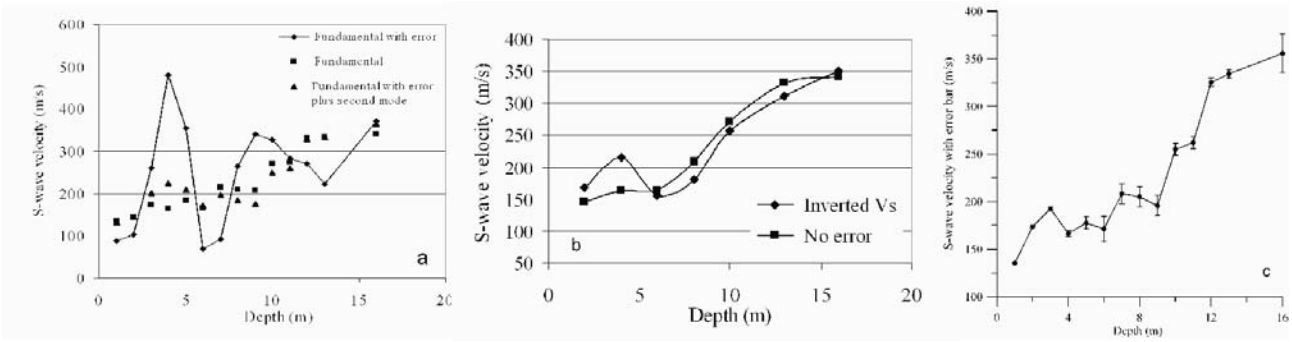

Figure 7. (a) Inverted S-wave velocity profiles from three data sets; (b) inverted S-wave velocity (labeled as "Inverted V_S") from data set "fundamental with error" using a 2-m layer thickness compared with inverted results (labeled as "No error") from the fundamental data with no error; (c) S-wave velocities determined by an extra iteration from the model inverted from data set "fundamental with error plus second mode" with error bars (from Xia et al., 2008b, 2003).

Appraisal of Inverted Model

Some researchers also noted that some data at certain frequencies within the same mode are more important than others in resolving S-wave velocities. Studies (Xia et al., 2008a) on the data-resolution matrix (Minster et al., 1974) of the inversion system of surface waves provided insight into the intrinsic characteristic that higher modes are normally predicted much more easily than the fundamental mode. The studies show that each near-surface geophysical target can only be resolved using Rayleigh-wave phase velocities within specific frequency ranges, and higher-mode data are normally more accurately predicted than fundamental-mode data because of restrictions on the data kernel for the inversion system. Xia et al. (2008a) used synthetic and real-world examples to demonstrate that selected data with the data-resolution matrix can provide better inversion results and to explain with the data-resolution matrix why incorporating higher-mode data in inversion can provide better results. They also calculated model-resolution matrices in these examples to show the potential of increasing model resolution with selected surface-wave data.

Appraisal of inverse models is essential to a meaningful interpretation of these models. Because uncertainties are associated with the damping factor, extra conditions are usually required to determine the proper parameters for assessing inverse models. To find the proper damping factor, Xia et al. (2008b) considered an objective function that is the trace of a weighted sum of model-resolution and model-covariance matrices in the vicinity of a regularized solution where the linearity of inverse problems is held. Using the singular-value decomposition, they derive explicit formulae to calculate a damping vector [the ith component is $\lambda_i = 0.5(\sqrt{\Lambda_i^4 + 4\Lambda_i^2} - \Lambda_i^2)$] and a weighting vector that results in a minimized objective function. With the optimum damping vector and weighting vector, we obtain a trade-off solution between model resolution and model covariance in the vicinity of a regularized solution. The unit covariance matrix can then be used to calculate an error bar of the inverse model with $\Delta m_i = \Delta d \sqrt{\sum_{j=1}^{n} \gamma_j v_{ij}^2}$, where Δm_i is the ith element of the standard deviation Δm of an inverse model; $\gamma_j = \Lambda^2{}_j (\Lambda^2{}_j + \lambda_j)^{-2}$; Λ_i is the ith singular value; v_{ij} is the element of matrix $\boldsymbol{V}$ (an $n \times n$ matrix after singular-value decomposition of a data kernel) at the ith row and the jth column; and Δd is the data standard deviation, which could be replaced by a threshold of terminating iterations. They calculated the error bar (Fig. 7c) associated with the results of the San Jose example.

SEISMIC MODELING AND HORIZONTAL RESOLUTION

Recent developments in seismic modeling and mode separation build a new basis for surface-wave techniques. Inversion of a full-wave field in near-surface setting becomes feasible with a current PC. Horizontal resolution could be dramatically improved

with the mode-separation technique.

Seismic Modeling

Inversion of surface waves or a full-wave field in the time-offset domain for near-surface material characterization is always an objective that attracts attention from the geophysics community. To build a basis for inversion, seismic modeling with a new implementation (Xu et al., 2007) has been developed for simulating elastic-wave propagation, where the free-surface condition is replaced by an explicit acoustic/elastic boundary. Detailed comparisons of seismograms with different implementations for the air/earth boundary were undertaken using the (2, 2) (the finite-difference operators are second-order in time and space) and the (2, 6) (second-order in time and sixth-order in space) standard staggered grid schemes.

High-frequency Rayleigh waves (Fig. 8a) due to a two-layer model were simulated using a finite-difference method (Xu et al., 2007). The model consists of the surface layer V_P=800 m/s, V_S=200 m/s, ρ= 2 000 kg/m^3, and thickness=10 m, and the half-space V_P=1 200 m/s, V_S =400 m/s, and ρ=2 000 kg/m^3. The dispersive energy of Rayleigh waves was clearly modeled in a synthetic shot gather with 60 channels (Fig. 8a). Figure 8b shows the dispersion image in the *f-v* domain generated by Luo et al. (2008a) with analytical results calculated by Knopoff's method (Schwab and Knopoff, 1972). A reason for the differences between the numerical results and Knopoff's calculated results (Fig. 8b) is the grid size (1 m by 1 m) used in the modeling. If a grid size of 0.25 m by 0.25 m was used, no difference could be visually noted.

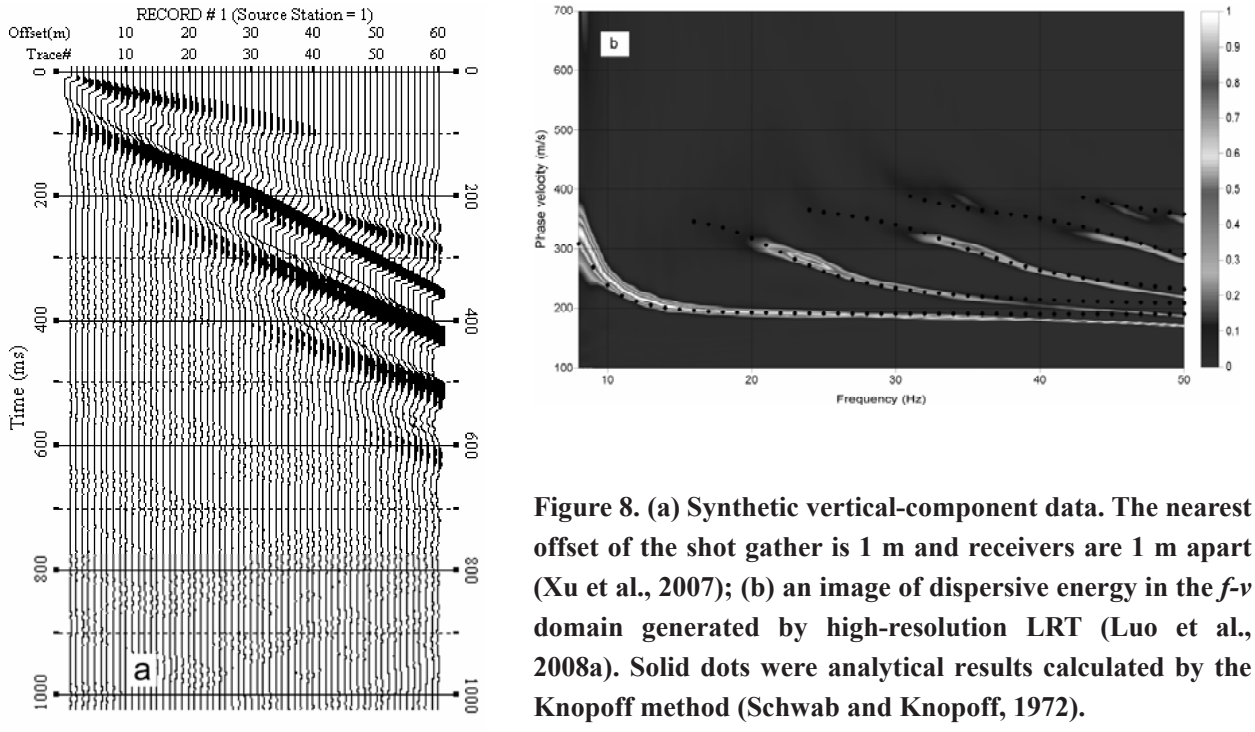

Figure 8. (a) Synthetic vertical-component data. The nearest offset of the shot gather is 1 m and receivers are 1 m apart (Xu et al., 2007); (b) an image of dispersive energy in the *f-v* domain generated by high-resolution LRT (Luo et al., 2008a). Solid dots were analytical results calculated by the Knopoff method (Schwab and Knopoff, 1972).

Horizontal Resolution

The MASW method attracted more attention in the near-surface geophysics community after it was used in subsurface mapping in the later 1990s. A technique (Xia et al., 2004a, b, 1998; Miller et al., 1999) combined the MASW method with a standard CMP (common middle point) roll-along acquisition format (Mayne, 1962) to generate pseudo-2D S-wave velocity sections. Inverting phase velocities from the MASW method give us an S-wave velocity profile (1-D S-wave velocity function, V_S vs. depth) at the center of a receiver spread. Because data are acquired in the standard CMP format, phase velocities of Rayleigh waves can be extracted from each shot gather so that numerous 1-D S-wave profiles along a survey line can be generated and placed at the center of each receiver spread (Luo et al., 2009a; Miller and Xia, 1999). A pseudo-2D vertical section of S-wave

velocity then can be generated by any contouring software. This technique possesses a very high potential for application in the urban environment due to its high signal-to-noise ratio (Xia et al., 2004a). Numerous successful applications of this method were introduced in the literature (e.g., Chen et al., 2006; Ivanov et al., 2006a, b; Tian et al., 2003a, b). However, because S-wave velocities derived from the MASW method are a kind of averaged value of the materials between the source (or the first receiver) and the last receiver or inversion based on an assumption of the layered-earth model, a process that reduces horizontal resolution, applications of the method in near-surface geophysics are limited. Understanding horizontal resolution, however, remains a challenge for subsurface mapping with the MASW method. Xia et al. (2005) applied the generalized inversion (Menke, 1984) to demonstrate that horizontal resolution can be improved by unblurring processing. However, the ultimate improvement of horizontal resolution should come from reducing the receiver spread.

Studies by Luo et al. (2008c, d) present a stable and practical way to increase horizontal resolution. Different modes of multichannel surface-wave data in the *f-v* domain can be accurately separated by high-resolution LRT, and single-mode surface-wave data, which are free from higher modes and body waves, can be regenerated in the time-offset domain. For example, the fundamental mode (Fig. 9a) can be extracted from the image (Fig. 8b) and then the shot gather (Fig. 9b) that possesses only the fundamental mode and is free from body waves can be generated in the time-offset domain by high-resolution LRT (Luo et al., 2008d). Luo et al. (2008b, d) demonstrated that it is feasible to extract dispersion curves with a pair of traces within a small distance in the reconstructed gather (Fig. 9b), which increases the horizontal resolution of subsurface mapping with the MASW method. With properly selected fundamental-mode Rayleigh waves in mode separation, the low-frequency dispersion possesses high accuracy (the relative error smaller than 10%) even with a pair of traces within a

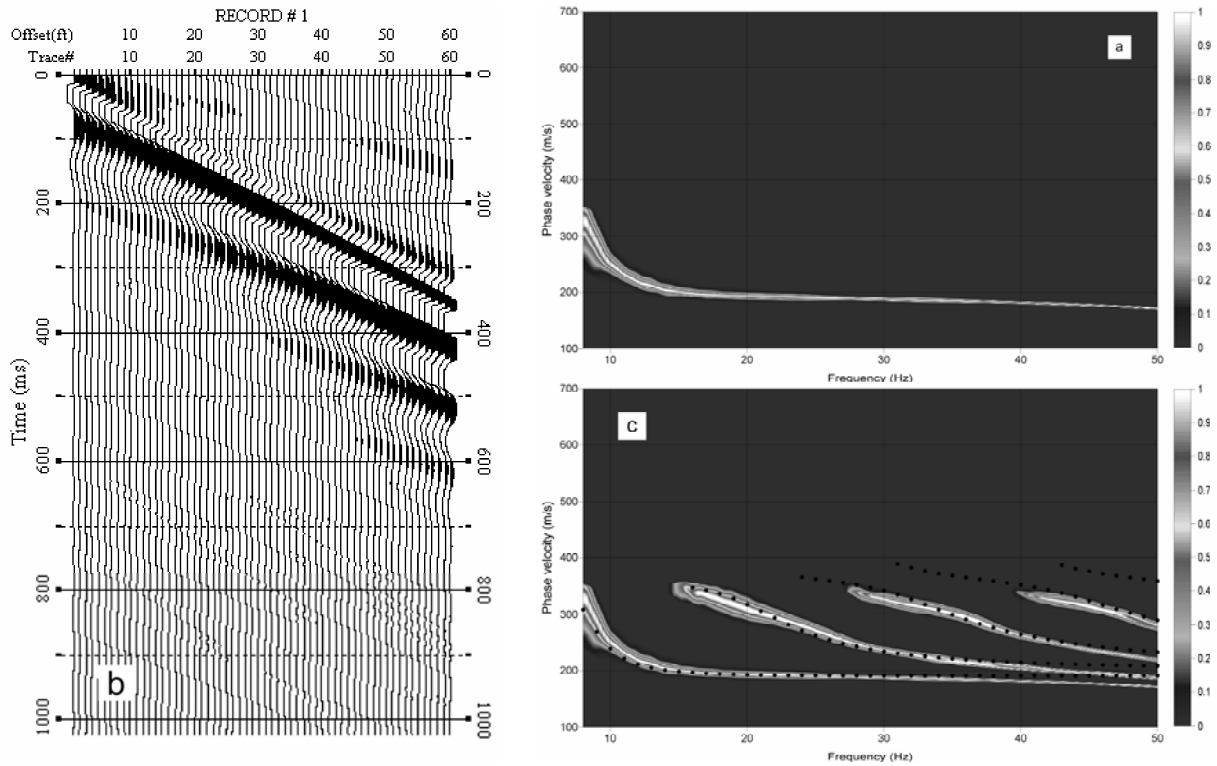

Figure 9. (a) An image of dispersive energy of the fundamental mode separated from Fig. 8b; (b) a shot gather that is calculated by applying high-resolution LRT to the image (a) and that possesses only the fundamental mode and is free from body waves (Luo et al., 2008c); (c) an image of dispersive energy of multimode surface waves generated by mode separation and reconstruction (Luo et al., 2008d).

small distance (Luo et al., 2008b, d).

After mode separation and reconstruction (Luo, et al., 2008d), a new dispersion image (Fig. 9c) of data (Fig. 8a) can be generated by superposing all modes. Compared with Fig. 8b, the reconstructed image (Fig. 9c) expands frequency ranges of higher modes, which increases a potential investigation depth and provides a means to accurately determine cut-off frequencies. By knowing the cut-off frequencies and the asymptotes at high frequencies and low frequencies, we are able to directly estimate the depth to the half-space, the S-wave velocities of surficial layer and the half-space, and distinguish higher modes from calculation artifacts in the *f*-*v* domain. Furthermore, we can cross-check inverted results (Xu et al., 2009; Xia et al., 2006a).

CONCLUSIONS AND FUTURE STUDIES

Field-data-acquisition parameters are directly related to an investigation depth of interest. Rules of thumb of determining the field-data-acquisition parameters that could maximize surface-wave energy in a record have been discussed. A high-resolution dispersion image generated by the high-resolution LRT produces phase velocities with confidence, especially at low frequencies, which is necessary for inversion that generates accurate S-wave velocities. Examples demonstrate that accurate S-wave velocities (±15%) can normally be obtained by inverting the fundamental mode of Rayleigh-wave phase velocities. The accuracy can be increased by inverting the fundamental mode with higher modes simultaneously. An inversion system of higher mode data produced the inverted model with even higher resolution. Inversion systems for S-wave velocities are numerically stable. It also is feasible to determine near-surface quality factors Q_S and/or Q_P from attenuation coefficients of Rayleigh waves. Regulated inverse results can be assessed with a trade-off solution between model resolution and model covariance matrices.

Seismic modeling by treating the free surface condition as an explicit acoustic/elastic boundary provides a tool to evaluate and study the seismic characteristics of near-surface features and builds a basis for full wavefield or Rayleigh-wave inversion in the time-offset domain. Successful separation of surface-wave modes makes it possible to perform high-resolution S-wave profiling with the MASW method in detecting or delineating small-scale geological features although horizontal resolution is not critical to defining large-scale geological features such as earthquake zonation (Yilmaz et al., 2006). Slant stacking (Xia et al., 2007a) possesses the capability to generate an image of dispersive energy from data acquired in an arbitrary acquisition geometry (for example, a fan configuration), which lays down a foundation for true 3D surface-wave analysis. Some research results on 3D surface-wave techniques are expected to be in referred literature in the near future.

Physical modeling of surface-wave response in various geological settings needs to be done for better understanding and verification of phenomena observed in numerical modeling. Few studies are available on determination of S-wave velocities from group velocities of Rayleigh waves. Group velocities may possess higher resolution than the phase velocities in the *f*-*v* domain, especially at low frequencies. Very limited publications exist in applying Love waves in near-surface geophysics, which may due to the difficulty of acquiring Love-wave data. Joint inversion of Rayleigh and Love waves could increase the reliability of S-wave velocity if objective functions are properly selected. Mapping specific near-surface features such as faults and voids using the MASW method is still a challenge. Current works are limited to some simple models. Surface-wave diffraction (Xia et al., 2007b) is of interest in the near-surface geophysics community. A few real-world examples (Putnam et al., 2008; Xia et al., 2007b) also show it is feasible to detect anomalous bodies in a shallow depth using surface-wave diffraction. Studies on the limitations of the MASW method have been reported in the literature. For example, Luo et al. (2009b) demonstrated using synthetic and real-world examples that a dipping interface with a slope smaller than 15 degrees can be successfully mapped by the separated fundamental mode using high-resolution LRT.

ACKNOWLEDGMENTS

The authors thank Marla Adkins-Heljeson of the Kansas Geological Survey for editing the manuscript. The authors also thank two anonymous reviewers for

their thorough review of the manuscript and constructive suggestions.

REFERENCES CITED

Abbiss, C. P., 1981. Shear Wave Measurements of the Elasticity of the Ground. *Géotechnique*, 31(1): 91–104

Babuska, V., Cara, M., 1991. Seismic Anisotropy in the Earth. Kluwer Academic Publishers, Boston. 217

Backus, G. E., Gilbert, J. F., 1970. Uniqueness in the Inversion of Inaccurate Gross Earth Data. *Phil. Trans. Roy. Soc. London*, *Ser.*, *A*, 266: 123–192

Beaty, K. S., Schmitt, D. R., Sacchi, M., 2002. Simulated Annealing Inversion of Multimode Rayleigh-Wave Dispersion Curves for Geological Structure. *Geophys. J. Int.*, 151(2): 622–631

Calderón-Macías, C., Luke, B., 2007. Addressing Nonuniqueness in Inversion of Rayleigh-Wave Data for Shallow Profiles Containing Stiff Layers. *Geophysics*, 72(1): U1–U10

Chen, C., Liu, J., Xia, J., et al., 2006. Integrated Geophysical Techniques in Detecting Hidden Dangers in River Embankments. *Journal of Environmental and Engineering Geophysics*, 11(2): 83–94

Clayton, C. R. I., 1993. The Standard Penetration Test (SPT): Methods and Use: Construction Industry Research and Information Association. Funder Report CP/7, London. 129

Clayton, C. R. I., Matthews, M. C., Simons, N. E., 1995. Site Investigation. Blackwell Science, Oxford. 584

Coruh, C., 1985. Stretched Automatic Amplitude Adjustment of Seismic Data. *Geophysics*, 50(2): 252–256

Dobry, R., Borcherdt, R. D., Crouse, C. B., et al., 2000. New Site Coefficients and Site Classification System Used in Recent Building Seismic Code Provisions. *Earthquake Spectra*, 16(11): 41–67

Dorman, J., Ewing, M., 1962. Numerical Inversion of Seismic Surface Wave Dispersion Data and Crust-Mantle Structure in the New York-Pennsylvania Area. *Journal of Geophysical Research*, 67(9): 3554

Forbriger, T., 2003. Inversion of Shallow-Seismic Wavefields: I. Wavefield Transformation. *Geophys. J. Int.*, 153(3): 719–734

Garland, G. D., 1979. Introduction to Geophysics: Mantle, Core and Crust. 2nd Edition. W. B. Saunders Company, Philadelphia. 494

Imai, T., Tonouchi, K., 1982. Correlation of N-Value with S-Wave Velocity and Shear Modulus. Proceedings of the Second European Symposium on Penetration Testing. 67–72

Ivanov, J., Miller, R. D., Lacombe, P., et al., 2006a. Delineating a Shallow Fault Zone and Dipping Bedrock Strata Using Multichannal Analysis of Surface Waves with a Land Streamer. *Geophysics*, 71(5): A39–A42

Ivanov, J., Miller, R. D., Xia, J., et al., 2006b. Joint Analysis of Refractions with Surface Waves: An Inverse Solution to the Refraction-Traveltime Problem. *Geophysics*, 71(6): R131–R138

Jin, S., Cambois, G., Vuilermoz, C., 2000. Shear-Wave Velocity and Density Estimation from PS-Wave AVO Analysis: Application to an OBS Dataset from the North Sea. *Geophysics*, 65(5): 1446–1454

Liang, Q., Chen, C., Zeng, C., et al., 2008. Inversion Stability Analysis of Multimode Rayleigh Wave Dispersion Curves Using Low-Velocity-Layer Models. *Near Surface Geophysics*, 6(3): 157–165

Lu, L., Wang, C., Zhang, B., 2007. Inversion of Multimode Rayleigh Waves in the Presence of a Low Velocity Layer: Numerical and Laboratory Study. *Geophys. J. Int*., 168(3): 1235–1246

Luo, Y., Xia, J., Liu, J., et al., 2007. Joint Inversion of High-Frequency Surface Waves with Fundamental and Higher Modes. *Journal of Applied Geophysics*, 62(4): 375–384

Luo, Y., Xia, J., Miller, R. D., et al., 2008a. Rayleigh-Wave Dispersive Energy Imaging by High-Resolution Linear Radon Transform. *Pure and Applied Geophysics*, 165(5): 903–922

Luo, Y., Xia, J., Liu, J., et al., 2008b. Generation of a Pseudo-2D Shear-Wave Velocity Section by Inversion of a Series of 1D Dispersion Curves. *Journal of Applied Geophysics*, 64(3–4): 115–124

Luo, Y., Xia, J., Miller, R. D., et al., 2008c. Rayleigh-Wave Dispersive Energy Imaging and Mode Separating by High-Resolution Linear Radon Transform. Proceedings of the 2008 International Conference on Environmental and Engineering Geophysics (ICEEG), June 15–20, Wuhan, China. 81–86

Luo, Y., Xia, J., Xu, Y., et al., 2008d. Rayleigh-Wave Dispersive Energy Imaging and Mode Separating by High-Resolution Linear Radon Transform. *The Leading Edge*, 27(11): 1536–1542

Luo, Y., Xia, J., Liu, J., et al., 2009a. Research on the Middle-of-Receiver-Spread Assumption of the MASW Method.

Soil Dynamics and Earthquake Engineering, 29(1): 71–79

Luo, Y., Xia, J., Xu, Y., et al., 2009b. Dipping Interface Mapping Using Mode-Separated Rayleigh Waves. *Pure and Applied Geophysics*, 166(3): 353–374

Marquardt, D. W., 1963. An Algorithm for Least Squares Estimation of Nonlinear Parameters. *Jour. Soc. Indus. Appl. Math*., 2: 431–441

Matthews, M. C., Hope, V. S., Clayton, C. R. I., 1996. The Use of Surface Waves in the Determination of Ground Stiffness Profiles. *Proc. Instn. Civ. Engrs.*, *Geotechnical Engineering*, 119: 84–95

Mayne, W. H., 1962. Horizontal Data Stacking Techniques. *Supplement to Geophysics*, 27: 927–937

McMechan, G. A., Yedlin, M. J., 1981. Analysis of Dispersive Waves by Wave Field Transformation. *Geophysics*, 46(6): 869–874

Menke, W., 1984. Geophysical Data Analysis—Discrete Inversion Theory. Academic Press, Inc., New York. 260

Miller, R. D., Xia, J., 1999. Feasibility of Seismic Techniques to Delineate Dissolution Features in the Upper 600 ft at Alabama Electric Cooperative's Proposed Damascus Site, Interim Report. Kansas Geological Survey, Open-File Report 99-3

Miller, R. D., Xia, J., Park, C. B., et al., 1999. Multichannel Analysis of Surface Waves to Map Bedrock. *The Leading Edge*, 18: 1392–1396

Minster, J. B., Jordan, T. J., Molnar, P., et al., 1974. Numerical Modeling of Instantaneous Plate Tectonics. *Geophys. J. Roy. Astron. Soc*., 36: 541–576

Moro, G. D., Pipan, M., Forte, E., et al., 2003. Determination of Rayleigh Wave Dispersion Curves for Near Surface Applications in Unconsolidated Sediments. Technical Program with Biographies, the 73rd Annual Meeting of the Society of Exploration Geophysicists, Dallas, TX. 1247–1250

Nazarian, S., Stokoe, K. H. II, Hudson, W. R., 1983. Use of Spectral Analysis of Surface Waves Method for Determination of Moduli and Thicknesses of Pavement Systems. *Transportation Research Record*, (930): 38–45

Park, C. B., Miller, R. D., Xia, J., 1998. Imaging Dispersion Curves of Surface Waves on Multi-channel Record. Technical Program with Biographies, the 68th Annual Meeting of the Society of Exploration Geophysicists, New Orleans, Louisiana. 1377–1380

Park, C. B., Miller, R. D., Xia, J., 1999. Multi-Channel Analysis of Surface Waves. *Geophysics*, 64(3): 800–808

Putnam, N., Nasseri-Moghaddam, A., Kovin, O., et al., 2008. Preliminary Analysis Using Surface Wave Methods to Detect Shallow Manmade Tunnels. Symposium on the Application of Geophysics to Environmental and Engineering Problems (SAGEEP), Annual Meeting of the Environmental and Engineering Geophysical Society (EEGS), April 6–10, 2008, Philadelphia, PA. 679–688

Rix, G. J., Leipski, A. E., 1991. Accuracy and Resolution of Surface Wave Inversion: Recent Advances in Instrumentation, Data Acquisition and Testing in Soil Dynamics. *Geotechnical Special Publication*, 29: 17–32

Rix, G. J., Lai, C. D., Spang, A. W. Jr., 2000. In Situ Measurement of Damping Ratio Using Surface Waves. *Journal of Geotechnical and Geoenvironmental Engineering*, 126(5): 472–480

Sabetta, F., Bommer, J., 2002. Modification of the Spectral Shapes and Subsoil Conditions in Eurocode 8. 12th European Conference on Earthquake Engineering: Paper Ref. 518

Schwab, F. A., Knopoff, L., 1972. Fast Surface Wave and Free Mode Computations. In: Bolt, B. A., ed., Methods in Computational Physics. Academic Press, New York. 87–180

Sêcoe, E., Pinto, P. S., 2002. Eurocode 8-Design Provisions for Geotechnical Structures. Special Lecture, 3rd Croatian Soil Mechanics and Geotechnical Engineering Conference, 2002 Hvar. CD-ROM

Sheriff, R. E., 2002. Encyclopedic Dictionary of Applied Geophysics. 4th Ed.. Society of Exploration Geophysicists, Tulsa, OK. 429

Sheriff, R. E., Geldart, L. P., 1983. Exploration Seismology (Volume 1): History, Theory, and Data Acquisition. Cambridge University Press, New York. 253

Song, X., Gu, H., 2007. Utilization of Multimode Surface Wave Dispersion for Characterizing Roadbed Structure. *Journal of Applied Geophysics*, 63(2): 59–67

Song, Y. Y., Castagna, J. P., Black, R. A., et al., 1989. Sensitivity of Near-Surface Shear-Wave Velocity Determination from Rayleigh and Love Waves. *Technical Program with Biographies*, *the 59th Annual Meeting of the Society of Exploration Geophysicists*, 59: 509–512

Steeples, D. W., Baker, G. S., Schmeissner, C., 1999. Toward the Autojuggie: Planting 72 Geophones in 2 Sec. *Geophysical Research Letters*, 26(8): 1085–1088

Stokoe, K. H. II, Nazarian, S., 1983. Effectiveness of Ground Improvement from Spectral Analysis of Surface Waves.

Proceeding of the Eighth European Conference on Soil Mechanics and Foundation Engineering, 1: 91–95

Stokoe, K. H. II, Wright, G. W., Bay, J. A., et al., 1994. Characterization of Geotechnical Sites by SASW Method. Geophysical Characterization of Sites. In: Woods, R. D., ed., ISSMFE Technical Committee #10, New Delhi. Oxford Publishers, Oxford. 15–25

Tian, G., Steeples, D. W., Xia, J., et al., 2003a. Useful Resorting in Surface Wave Method with the Autojuggie. *Geophysics*, 68(6): 1906–1908

Tian, G., Steeples, D. W., Xia, J., et al., 2003b. Multichannel Analysis of Surface Wave Method with the Autojuggie. *Soil Dynamics and Earthquake Engineering*, 23(3): 243–247

Tokimatsu, K., Kuwayama, S., Tamura, S., et al., 1991. V_s Determination from Steady State Rayleigh Wave Method. *Soils and Foundations*, 31(2): 153–163

Vardoulakis, I., Verttos, C., 1988. Dispersion Law of Rayleigh-Type Waves in a Compressible Gibson Half-Space. *International Journal for Numerical and Analytical Methods in Geomechanics*, 12(6): 639–655

Xia, J., Miller, R. D., Park, C. B., 1998. Construction of Vertical Section of Near-Surface Shear-Wave Velocity from Ground Roll. Technical Program, the Society of Exploration Geophysicists and the Chinese Petroleum Society Beijing 98' International Conference. 29–33

Xia, J., Miller, R. D., Park, C. B., 1999. Estimation of Near-Surface Shear-Wave Velocity by Inversion of Rayleigh Wave. *Geophysics*, 64(3): 691–700

Xia, J., Miller, R. D., Park, C. B., 2000. Advantages of Calculating Shear-Wave Velocity from Surface Waves with Higher Modes. *Technical Program with Biographies*, *the 70th Annual Meeting of the Society of Exploration Geophysicists*, 70: 1295–1298

Xia, J., Miller, R. D., Park, C. B., et al., 2002a. Comparing Shear-Wave Velocity Profiles Inverted from Multichannel Analysis of Surface Wave with Borehole Measurements. *Soil Dynamics and Earthquake Engineering*, 22(3): 181–190

Xia, J., Miller, R. D., Park, C. B., et al., 2002b. A Pitfall in Shallow Shear-Wave Refraction Surveying. *Journal of Applied Geophysics*, 51(1): 1–9

Xia, J., Miller, R. D., Park, C. B., et al., 2002c. Determining *Q* of Near-Surface Materials from Rayleigh Waves. *Journal of Applied Geophysics*, 51(2–4): 121–129

Xia, J., Miller, R. D., Park, C. B., et al., 2003. Inversion of High Frequency Surface Waves with Fundamental and Higher Modes. *Journal of Applied Geophysics*, 52(1): 45–57

Xia, J., Chen, C., Li, P. H., et al., 2004a. Delineation of a Collapse Feature in a Noisy Environment Using a Multichannel Surface Wave Technique. *Géotechnique*, 54(1): 17–27

Xia, J., Miller, R. D., Park, C. B., et al., 2004b. Utilization of High-Frequency Rayleigh Waves in Near-Surface Geophysics. *The Leading Edge*, 23(8): 753–759

Xia, J., Chen, C., Tian, G., et al., 2005. Resolution of High-Frequency Rayleigh-Wave Data. *Journal of Environmental and Engineering Geophysics*, 10(2): 99–110

Xia, J., Xu, Y., Chen, C., et al., 2006a. Simple Equations Guide High-Frequency Surface-Wave Investigation Techniques. *Soil Dynamics and Earthquake Engineering*, 26(5): 395–403

Xia, J., Xu, Y., Miller, R. D., et al., 2006b. Estimation of Elastic Moduli in a Compressible Gibson Half-Space by Inverting Rayleigh Wave Phase Velocity. *Surveys in Geophysics*, 27(1): 1–17

Xia, J., Xu, Y., Miller, R. D., 2007a. Generating Image of Dispersive Energy by Frequency Decomposition and Slant Stacking. *Pure and Applied Geophysics*, 164(5): 941–956

Xia, J., Nyquist, J. E., Xu, Y., et al., 2007b. Feasibility of Detecting Near-Surface Feature with Rayleigh-Wave Diffraction. *Journal of Applied Geophysics*, 62(3): 244–253

Xia, J., Miller, R. D., Xu, Y., 2008a. Data-Resolution Matrix and Model-Resolution Matrix for Rayleigh-Wave Inversion Using a Damped Least-Square Method. *Pure and Applied Geophysics*, 165(7): 1227–1248

Xia, J., Xu, Y., Miller, R. D., 2008b. Improvement and Assessment of a Damped Least-Square Solution of Rayleigh-Wave Inversion. Proceedings of the 2008 International Conference on Environmental and Engineering Geophysics (ICEEG), June 15–20, Wuhan, China. 20–28

Xu, Y., Xia, J., Miller, R. D., 2006. Quantitative Estimation of Minimum Offset for Multichannel Surface-Wave Survey with Actively Exciting Source. *Journal of Applied Geophysics*, 59(2): 117–125

Xu, Y., Xia, J., Miller, R. D., 2007. Numerical Investigation of Implementation of Air-Earth Boundary by Acoustic-Elastic Boundary Approach. *Geophysics*, 72(5): SM147–SM153

Xu, Y., Xia, J., Miller, R. D., 2009. Approximation to Cutoffs of Higher Modes of Rayleigh Waves for a Layered Earth Model. *Pure and Applied Geophysics,* 166(3): 339–351

Yilmaz, Ö., 1987. Seismic Data Processing. Society of Exploration Geophysicists, Tulsa, OK. 526

Yilmaz, Ö., Eser, M., Berilgen, M., 2006. A Case Study of Seismic Zonation in Municipal Areas. *The Leading Edge*, 25(3): 319–330

Zhang, S. X., Chan, L. S., Xia, J., 2004. The Selection of Field Acquisition Parameters for Dispersion Images from Multichannel Surface Wave Data. *Pure and Applied Geophysics*, 161: 185–201